Experimental study of polymer distributed feedback lasers

Tianrui Zhai (翟天瑞), Xinping Zhang (张新平)*, Zhaoguang Pang (庞兆广), and Hongmei Liu (刘红梅)

Institute of Information Photonics Technology and College of Applied Sciences, Beijing University of Technology, Beijing 100124, China

**Corresponding author: zhangxinping@bjut.edu.cn*

Received December 22, 2011; accepted February 21, 2012; posted online June 20, 2012

Different distributed feedback (DFB) configurations in optically pumped polymer lasers, including the active Bragg grating structures, the dielectric grating structures spin-coated with polymeric semiconductors, and the actively waveguide dielectric grating structures (AWGS), are studied systematically. In the experiment, the F8BT polymer poly [(9,9- dioctylfluorenyl-2,7-diyl)-alt-co- (1,4-benzo-{2,1',3} -thiadiazole)] is employed as the active medium in the three laser configuration. And all grating structures are fabricated though interference lithography or interference ablation. It is found that the AWGS design has advantages over the other two. The continuous and high-quality active waveguide in the AWGS enables low-threshold (115 μJ/cm^2) laser emission with narrow linewidth (~0.4 nm at full-width at half-maximum). The experimental verifications are in good agreement with the theoretical analysis. These results reveal some interesting mechanisms in optically pumped DFB polymer lasers, and it may be enlightening to the construction of electrically driven organic lasers.

OCIS codes: 140.3490, 160.5470, 260.3160.

doi: 10.3788/COL201210.S11409.

Since the pioneering contributions of Moses[1], organic semiconductor lasers, especially optically pumped polymer lasers have been studied extensively[2−4]. The distributed feedback (DFB) structures are the most promising configurations for constructing the cavities of polymer lasers[5−7]. Three kinds of DFB cavities are commonly employed, the polymer Bragg grating structures[8−10], the dielectric grating structures spin-coated with the polymer[11−13] and the actively waveguide grating structures (AWGS)[14]. The DFB cavities can be fabricated by UV embossing[5], micromolding[15], electron beam lithography[16], or reactive ion etching[13]. In this letter, we systematically compare polymer lasers with three kinds of DFB cavities using interference ablation and interference lithography.

Figure 1 shows the design of three DFB cavities for the realization of surface-emitting polymer lasers. Figures 1(a)–(c) depict the polymer Bragg grating structure, the dielectric grating structure spin-coated with the polymer and the AWGS, respectively.

In the experiment, the F8BT polymer semiconductor: poly[(9,9-dioctylfluorenyl-2,7-diyl)-alt-co-(1,4-benzo-{2,1',3}-thiadiazole)] (American Dye Source, Inc) is employed as the active medium[14]. The solution of F8BT in chloroform with a concentration of 20 mg/ml is spin-coated onto the dielectric grating structure (Fig. 1(b)) or the glass substrate (Figs. 1(a), (c)) with an area of 20×20 (mm) and a thickness of 1 mm, forming high-quality thin film with a thickness of about 200 nm. The grating structure are fabricated using interference ablation (Fig. 1(a)) and interference lithography (Figs. 1(b) and (c)), which are written directly into the polymer (Fig. 1(a)) or the photoresist (PR, Figs. 1(b) and (c)) (S1 805, Rohm & Haas) with a period of 350 nm. A diode-pumped frequency-tripled (355 nm) solid-state laser (Advanced Optical Technology Ltd.) with a pulse length of 500 ps and a repetition rate of 6.25 kHz is employed to perform the interference lithography and to pump the polymer laser. And a frequency-quadrupled (266 nm) diode-pumped solid-state laser (Innolas, Spitlight 200) with a pulse length of 6 ns and a pulse energy of 20 mJ is employed as laser source for the interference ablation. The upper panel in Fig. 2 shows the experimental setup for interference ablation and interference lithography. The UV laser pulse at 266 nm (for interference ablation) or 355 nm (for interference lighography) is split into two beams before being overlapped onto the thin-film sample. The angle α between the two UV laser beams is changed to control the periods Λ of the grating structures by a relation of $\Lambda = \frac{\lambda}{2\sin(\alpha/2)}$, where λ is the wavelength of the UV laser. Figure 2 shows the atomic force microscopic image (measured by Agilent 5 500) of the laser sample, which corresponds to the grating structure made by interference ablation (Fig. 2(a)) and interference lithography (Fig. 2(b)).

Laser pulses at 355 nm are used as the pump source, which are incident onto the sample at an angle of about 20° after being focused by a lens with a focal length of 100 mm. The spot size of the pump laser on the

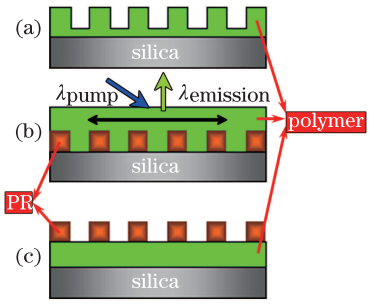

Fig. 1. Design of three kinds of DFB cavities. Figures 1(a)–(c) depict the polymer Bragg grating structure, the dielectric grating structure spin-coated with the polymer, and the AWGS, respectively. Arrows in Fig. 1(b) shows the schematic diagram of all surface-emitting DFB polymer laser structures.

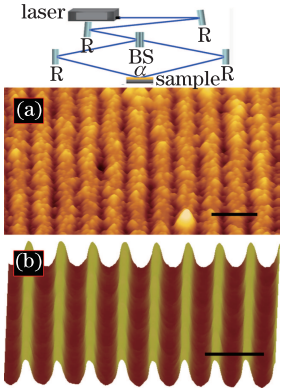

Fig. 2. AFM images of the grating structure made by (a) interference ablation and (b) interference lithography. The black bars denote 1 μm. The upper panel denotes the experimental setup for interference ablation and interference lithography.

laser sample is estimated to be about 200 μm in radius. The pump pulse energy is controlled by sending the laser beam through an attenuator wheel. Figures 3(a)–(c) show the photographs of the laser action based on different structures depicted in Figs. 1(a)–(c), respectively. A strip consisting of two arc lines can be observed for the laser device. Most of the laser energy is focused into the center area of the spot. The horizontal profile of the laser beam is defined by the Bragg diffraction of the DFB structures. It can be seen that the radiation energy of the polymer laser based on AWGS is confined almost completely in the center of the vertical rainbows (Fig. 3(c)), implying much improved transverse mode as compared with that in the design of Figs. 1(a) and (b). A comparison is made for the transverse modes measured at the same distance from the laser configuration shown in Figs. 1(a)–(c). The half divergence angles of the beam from the laser design shown in Figs. 1(a)–(c) are measured to be about 3°, 2°, and 0.44°, respectively, which implies significantly improved transverse mode by the AWGS configuration.

The characterization of the laser output influences the performance of the laser device. Therefore, the spectroscopic characterizations of the output of different polymer lasers (Figs. 1(a)–(c)) are shown in Fig. 4, where Fig. 4(b) summarizes the spectral intensity of the laser emission as a function of the pump fluence. For the configurations shown in Figs. 1(a)–(b), the laser emission are centered at about 569 nm in the spectrum and has a bandwidth of about 1.3 nm at full-width at half-maximum (FWHM), while for the configuration shown in Fig. 1(c), the laser emission is centered at 564 nm and has FWHM of about 0.4 nm. The spectra are measured with an Ocean optics Maya 2 000 PRO spectrometer, which has a resolution of 0.2 nm. Therefore, the practical spectral linewidth of the laser emission is smaller. The narrow linewidth implies excellent oscillation modes in the DFB cavity based on AWGS shown in Fig. 1(c). As can be evaluated using Fig. 4(b), the pump threshold of three laser configurations shown in Figs. 1(a)–(c) are about 130, 150, and 115 μJ/cm^2, respectively. And the largest output slope of the AWGS shown in Fig. 4(b) also indicates the DFB structure based on AWGS enable more efficient operation of the laser device.

For all DFB configurations, the resonance condition satisfies the equation of $\Lambda = m\lambda_{\rm eff}/2$, where Λ is the period of the grating, m is the order of the cavity mode, $\lambda_{\rm eff} = \lambda_0/n_{\rm eff}$ is the DFB effective wavelength, λ_0 is the wavelength of the polymer laser emission, $n_{\rm eff}$ is the effective index of the active medium. The surface-emitting polymer laser based on the grating structures corresponds to the second order Bragg mode (m=2). So, the effective index of the active medium can be estimated by $n_{\rm eff} = \lambda_0/\Lambda$. In our experiment, the effective index of the DFB configuration shown in Figs. 1(a)–(c) are 1.63, 1.63, and 1.61, respectively.

From the experimental results of different DFB configuration shown in Fig. 1, it can be concluded that the most notable feature of Fig. 1(a) is simple production: one pulse, one sample. While Fig. 1(c)

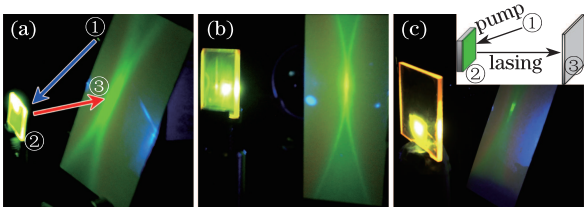

Fig. 3. (Color online) Photographs of the operating polymer laser based on different mechanisms shown in Fig. 1. The blue/red arrow denotes the incident/surface-emitting laser, respectively. The pump laser is designed by ①. The sample is designed by ②. The white screen is designed by ③. The inset in (c) depicts the light path.

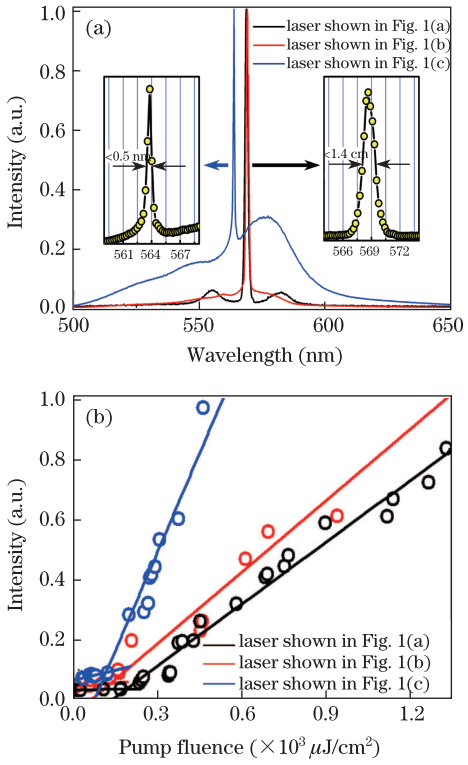

Fig. 4. (a) Measured spectra of the lasing emission of different DFB configurations. The left/right panel is the enlarged view of the blue/black line. (b) Output intensity of different polymer lasers as a function of the pump fluence, indicating pump thresholds of 130, 150, and 115 μJ/cm^2 for laser configurations shown in Figs. 1(a)–(c), respectively.

has more advantages in laser performance, which lies the following aspects: (1) High-quality thin film of the active materials is produced without being modulated by the grating structures, ensuring narrow linewidth of the laser emission. (2) AWGS configuration enables the most efficient utilization of the active volume, ensuring low operating threshold. (3) AWGS configuration facilitates stronger confinement, ensuring a small divergence angle of the laser beam. (4) AWGS is insensitive to the defects or inhomogeneity in the grating structures.

To examine the advantages of the AWGS configuration, we do some full wave simulations using the finite-element method. It can be seen that the eigen modes are distributed partially in the active waveguide in Figs. 5(a)-(b). However, for the AWGS configuration, the field distribution of the eigen mode is confined almost completely in the active waveguide layer (Fig. 5(c)), which is consist with its first three advantages. In the simulations, the polymer layer ($n_{\rm polymer}$=1.8) has a thickness of 200 nm, and the PR grating ($n_{\rm PR}$=1.67) has a period of 350 nm and a modulation depth of 200 nm. The substrate is made of silica ($n_{\rm silica}$=1.5) and the medium on top of the laser device is air ($n_{\rm air}$=1.0).

Also, we note that the DFB configuration that the conjugated polymer is spin-coated onto the grating structures and more sensitive to the defects in the grating structures. Figure 6 compares the sensitivity of different cavity configurations shown in Fig. 1 to the similar defects in the grating structures. It can be seen clearly that any defects or inhomogeneity of the grating structures may destroy the mechanisms for DFB in the laser design. However, for the AWGS and the polymer grating structure, the DFB mechanisms are almost not disturbed.

In conclusion, we study the laser radiation mechanisms of the polymer lasers employing different distributed feedback designs. The AWGS structure is demonstrated as a new DFB configuration that favors better laser performance, which is based on the homogeneous layer of the active medium without being modulated spatially. This kind of configuration of the laser device possesses a number of advantages, which are verified both by theoretical simulations and by the experimental results.

This work was supported by the National Natural Science Foundation of China (Nos. 11074018 and 11104007), the Program for New Century Excellent Talents in University (NCET), the Research Fund for the Doctoral Program of Higher Education of China (No. 20091103110012), the Beijing Postdoctoral Research Foundation (No. 2011ZZ-22), and the Beijing Educational Commission (No. KM201210005034).

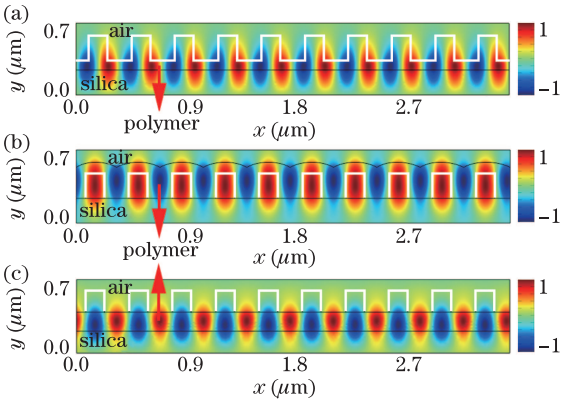

Fig. 5. (Color online) Eigen modes (electric field) of the DFB design with (a) the polymer grating structure, (b) the active layer spin-coated on top of the grating structures, and (c) the AWGS. The color spots denote the TE electric distribution.

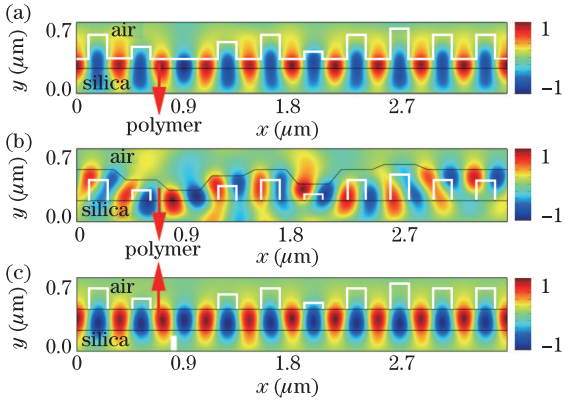

Fig. 6. (Color online) Response to the defects in the grating structures of (a) the polymer grating structure, (b) the active layer spin-coated on top of the grating structures, and (c) the AWGS. The color spots denote the TE electric distribution.

References

1. D. Moses, Appl. Phys. Lett. **55,** 22 (1993).
2. N. Tessler, G. Denton, and R. Friend, Nature **382,** 695 (1996).
3. F. Hide, M. Diaz-Garcia, B. Schwartz, M. Andersson, Q. Pei, and A. Heeger, Science **273,** 1833 (1996).
4. W. Holzer, A. Penzkofer, S. Gong, A. Bleyer, and D. Bradley, Adv. Mater. **8,** 974 (1996).
5. M. Berggren, A. Dodabalapur, R. Slusher, A. Timko, and O. Nalamasu, Appl. Phys. Lett. **72,** 410 (1998).
6. H. Kogelnik and C. Shank, J. Appl. Phys. **43,** 2327 (1972).
7. T. Zhai, X. Zhang, Z. Pang, X. Su, H. Liu, S. Feng, and L. Wang, Nano Lett. **11,** 4295 (2011).
8. J. Herrnsdorf, B. Guilhabert, Y. Chen, A. Kanibolotsky, A. Mackintosh, R. Pethrick, P. Skabara, E. Gu, N. Laurand, and M. Dawson, Opt. Express **18,** 25535 (2010).
9. M. Gaal, C. Gadermaier, H. Plank, E. Moderegger, A. Pogantsch, G. Leising, and E. List, Adv. Mater. **15,** 1165 (2003).
10. T. Zhai, X. Zhang, Z. Pang, and F. Dou, Adv. Mater. **23,** 1860 (2011).
11. V. Navarro-Fuster, E. Calzado, P. Boj, J. Quintana, J. Villalvilla, M. Díaz-García, V. Trabadelo, A. Juarros, A. Retolaza, and S. Merino, Appl. Phys. Lett. **97,** 171104 (2010).
12. G. Heliotis, R. Xia, G. Turnbull, P. Andrew, W. Barnes, I. Samuel, and D. Bradley, Adv. Funct. Mater. **14,** 91 (2004).
13. G. Turnbull, P. Andrew, M. Jory, W. Barnes, and I. Samuel, Phys. Rev. B **64,** 125122 (2001).
14. T. Zhai, X. Zhang, and Z. Pang, Opt. Express **19,** 6487 (2011).
15. J. Lawrence, G. Turnbull, and I. Samuel, Appl. Phys. Lett. **82,** 4023 (2003).
16. M. Salerno, G. Gigli, M. Zavelani-Rossi, S. Perissinotto, and G. Lanzani, Appl. Phys. Lett. **90,** 111110 (2007).